7th International Symposium on Marine Propulsors
smp'2022, Wuxi, China, October 17-21, 2022

Towards Reliable Prediction of Propeller Noise: Challenges and Findings of the Project ProNoVi

Vladimir Krasilnikov[1], Luca Savio[1], Kourosh Koushan[1], Mario Felli[2], Moustafa Abdel-Maksoud[3], Julian Kimmerl[4], Nils Reichstein[5], Arve Fageraas[6], Jessica Sun[6]

[1]SINTEF Ocean, Ships and Ocean Structures, Trondheim, Norway
[2]CNR INM, Rome, Italy
[3]Technical University Hamburg (TUHH), Hamburg, Germany
[4]SCHOTTEL GmbH, Dörth, Germany
[5]Fr. Lürssen Werft GmbH & Co KG, Bremen-Vegesack, Germany
[6]Helseth AS, Hjelset, Norway

ABSTRACT

The present paper gives an overview of the research scope of the project ProNoVi targeting improvements in the methods to predict noise and vibration induced by marine propellers. The paper describes contents of the performed experimental campaign, developed validation datasets, and application of high-fidelity numerical approaches to practical calculation of hydroacoustic performance of propellers operating in open water conditions and behind ship hull. Comparisons are presented between the numerical predictions and experimental measurements on a reference ship case, for selected conditions, and challenges encountered during validation are discussed.

Keywords

Underwater Radiated Noise, Cavitation, Two-Phase Flow, CFD, Propulsion

1 INTRODUCTION

In the global picture of the quest to reduce environmental impact from shipping, underwater radiated noise is recognized as a harmful form of pollution to marine ecosystem (IMO, 2014). Originating from different sources (engine, propellers, hull vibration, boundary layer) the sound spectrum of ships covers the range of frequencies from 10Hz to 4kHz. However, it is the low frequencies between 100Hz and 300Hz dominated by propeller cavitation that cause greatest concern regarding the impact on communication and natural behavior of certain marine species (Cruz et al., 2021). It is estimated that, in this range, the background noise level in the oceans is raised with the rate of over 3dB per decade because of shipping. Traditionally viewed from the standpoint of long-distance sea transportation, today this problem is seen in a broader context due to intensified coastal activities related to renewable energies and aquaculture markets.

This paper presents a summary of challenges and main findings of the project ProNoVi (Kimmerl et.al., 2019), (http://www.pronovi.eu) which has been carried out in the period between June 2018 and November 2021 and funded by the ERA-NET Cofund MarTERA program, call 2017. The primary scientific goal of the project ProNoVi was to make progress beyond state-of-the-art in theoretical understanding and practical simulation of complex, multi-disciplinary problem of ship and propeller hydroacoustics. To this end, the project employed advanced experimental techniques, both in model scale and full scale, to predict propeller noise levels on the reference ship and to collect accurate data for the validation of numerical methods, including high-fidelity CFD solutions and practical engineering tools that can be used at early design phases. The developed approaches were applied to several target cases of ships and propulsion systems selected by the industrial partners in the project.

The two consortium partners, SINTEF Ocean and CNR INM, have conducted an extensive experimental campaign with the reference ship case, a twin-screw yacht equipped with shaft propellers. Two propeller designs were studied, one of which (open geometry) was produced specifically for the purpose of the present test campaign and designed to exhibit different types of cavitation. The test program featured observations of cavitation (high-resolution photography, high-speed video, cavitation diagram and stereometry for selected conditions), measurements of hull pressure pulses, noise measurements, and detailed flow measurements around propeller and rudder. The same test conditions were reproduced at the two testing facilities to replicate the conditions of full-scale trials conducted by Lürssen.

On the numerical side, the research conducted by SINTEF Ocean, SCHOTTEL and Helseth has highlighted the importance of employing Scale Resolving CFD Simulations, such as Detached Eddy Simulation (DES) and Large Eddy Simulation (LES) to achieve the level of fidelity required for an adequate resolution of salient flow features

behind propeller noise generation. Using these methods for hydrodynamic noise sources and the Ffowcs Williams-Hawkings method with permeable emission surface (P-FWH) for acoustic propagation, one achieves good agreement between the noise calculations using acoustic analogy and direct noise calculation by CFD in the near field. A satisfactory agreement with experimental noise measurements is also documented in the most relevant range of low frequencies. In parallel, to facilitate faster engineering calculations of propeller's acoustic performance, a set of design-oriented tools has been developed in ProNoVi by TUHH based on the Artificial Neural Network (ANN) solutions, and a coupled RANS-BEM approach which also implement the P-FWH method of acoustic analogy. In this paper, the authors focus on describing the contents of the performed experimental campaign, developed validation datasets, and their experience with Scale Resolving CFD method to practical calculation of propeller induced noise and pressure fluctuations. Comparisons are presented between the numerical predictions and experimental measurements on the reference ship case, for selected conditions, challenges encountered during validation are discussed, and directions of future research are outlined.

2 METHODS

In this section, the experimental and numerical approaches employed in ProNoVi to predict propeller induced noise and pressure fluctuations on ship hull are described.

2.1 Experimental methods

Within the work package regarding experimental methods, SINTEF Ocean and CNR INM have conducted an extensive experimental campaign with the reference target ship case, a twin-screw yacht equipped with shaft propellers. The experimental campaigns in both facilities included tests with an isolated propeller (without ship hull or, conditionally, in open water) in straight flow and on inclined shaft, and tests with propeller operating behind ship hull, with and without rudder. The test matrices covered a broad range of operation conditions with respect to propeller loading and cavitation number. The main test programs carried out by both institutions featured observations of cavitation (high-resolution photography, high-speed video), hull pressure pulse measurements, and noise measurements. Separately, detailed flow measurements, including conditions with operating propeller, were conducted by CNR INM. SINTEF Ocean performed tests to define propeller cavitation diagrams and stereometry for selected conditions, and they tested an additional propeller model designed specifically for ProNoVi test campaign. It is particularly important that the same test conditions for behind hull tests were reproduced at the two different facilities – the large cavitation tunnel of SINTEF Ocean and the large free-surface cavitation water channel of INM – thus allowing to assess the influence of facility and analysis procedures on the measurements in model scale and their extrapolation to full-scale conditions. Among other aspects is the effect of reverberation, which is inherent to all sound measurements performed in confined environments, and which is manifested in so-called "cut-off" frequency which depends on the facility type and size. In the case of SINTEF Ocean cavitation tunnel, the said "cut-off" frequency is estimated around 1000 (Hz), while for the Large Cavitation Channel of CNR INM it is 600 (Hz). For the same target ship case, the measurements of pressure pulses and radiated noise in full-scale were conducted by L ürssen.

The measurements by CNR INM are conducted in the institute's Large Cavitation Channel with dimensions of 10m×3.6m×2.25m at the test section, on a full hull model as shown in Fig. 1 for the case of behind hull tests. The setup consisted of 2 hydrophones (H1 and H2) positioned in correspondence of the propeller plane with H1 located 112cm beside the propeller axis on the starboard side, and H2 located 140cm below the propeller axis in correspondence of the facility midplane.

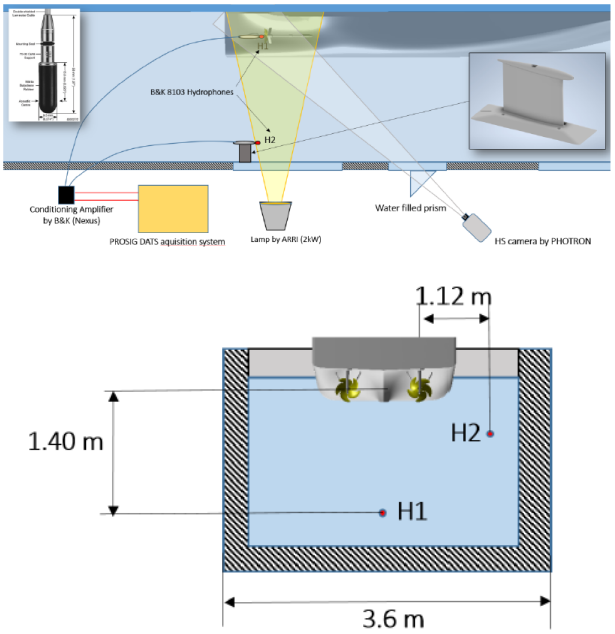

Figure 1. Experimental setup used in propeller behind hull tests at CNR INM

The hydrophones are miniature, high-sensitivity transducers by Brüel & Kjær of the model B&K 8103 with the frequency range of 0.1Hz÷180 kHz and sensitivity of 211dB re 1V/µPa. Hydrophone signals are conditioned by a Brüel & Kjær "NEXUS" charge amplifier and then acquired by a 20-channel/24-bit DAW PROSIG P8200. Additionally, 9 pressure gauges were located on the hull as indicated in Fig. 2. These are the dynamic pressure transducers PCB 106B with the frequency range of 0.5Hz÷60kHz and sensitivity of 43.5mV/kPa, flush mounted to the hull vault through dedicated metallic inserts. Pressure signals are recorded for the time window of ΔT=90s at the sampling frequency of 100kHz.

Cavitation observations were performed through a high-speed camera by Photron (Photron SAx1 model), rotated by 45 ° along the vertical axis directed at the starboard

propeller from one side through a 45 °inclined water prism attached to the facility window. The illumination is provided by a 1800W high-intensity HMI lamp by ARRI and a 1000W halogen lamp by DEDOLIGHT.

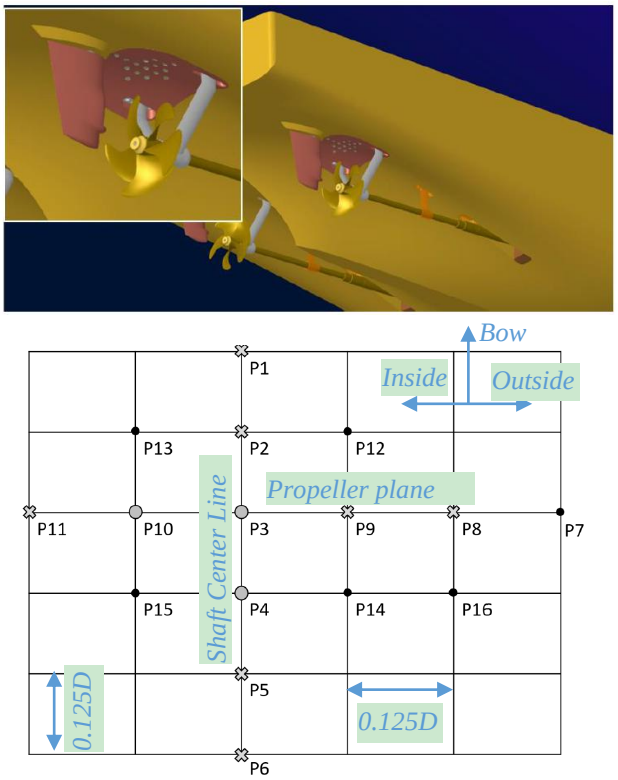

Figure 2. Arrangement of pressure transducers on ship hull

For the experimental results, transfer functions are calculated with background noise measurements, which are applied to the propeller measurements, in order to obtain propeller net noise.

At SINTEF Ocean tests were carried out in the Large Cavitation Tunnel with the length of the test section L=6m, and cross-section dimensions W×H=1.3m×1.2m. The behind hull tests were performed with a half-ship model. The port side of the model was manufactured and installed inside the test section of the cavitation tunnel with the model center plane attached to the test section side wall. A horizontal wooden plate was substituting the water free surface. The mentioned plate was not placed at the exact water line level but in such a way that it allowed to fit the model inside the tunnel and to measure the wake field on the propeller plane using the LDV equipment mounted in correspondence of the side window beside the propeller plane. Fig. 3 shows the arrangement of the hull model in the cavitation tunnel at SINTEF Ocean and the arrangement of hull pressure transducers which is identical to that used in CNR INM's tests. The rudder was designed removable to enable model tests with and without rudder blade installed. The acquisition of the propeller induced hull pressure pulses was conducted at 9.6 kHz with an applied filter having a cut-off frequency of 2.0 kHz.

One hydrophone (type Broeel & Kjaer model 8103) was used to measure the underwater sound pressure levels. The hydrophone was housed in a hydrofoil located inside the cavitation test section positioned at the distance of

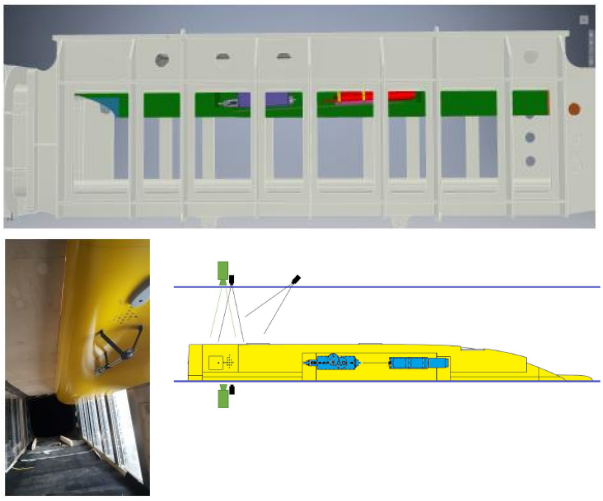

Figure 3. Experimental setup used in propeller behind hull tests at SINTEF Ocean

0.374 m from the propeller center (dX = 95 mm in front of propeller center; dY = 37 mm towards the ship side; dZ = 360 mm below the propeller center). Hydrophone signals were recorded at the frequency of 96.0 kHz.

Three video camera locations were used to observe and document the tests. Two of these locations allowed to look at the propeller from port side, from bow-quartering, and beam angle with respect to the propeller plane allowing to spot back cavitation. The last camera location allowed to look through the model skeg and visualize the blade's face side with the propeller blades in positions between 12 and 3 o'clock. The schematic view of camera installation layout is shown in Fig. 3, where the photo-cameras are shown in black symbols. A high-speed camera was also adopted to record high-speed videos at the frame rate of 2000 Hz capturing a frame at the interval of 6 degrees of propeller rotation. The high-speed cameras were used at two locations as shown in Fig. 3 by green symbols. Such detailed video recordings permit highly accurate visualization of unsteady flow mechanisms related for example to the interaction between the propeller tip and hub vortices, or mitigating effect of a specially designed rudder bulb on the strength of propeller hub vortex as illustrated in Figs. 4 and 5, respectively.

Detailed flow measurements were performed by CNR INM using a two-component back-scatter Laser Doppler Velocimeter (LDV). The LDV probe works in a backscatter mode and allows measuring up to two orthogonal velocity components simultaneously. The 3D velocity field was reconstructed using three optical configurations and two probe configurations, more specifically: (i) The probe configuration with the laser beams coming from a side was used to measure the axial and the vertical velocity components (U and W); (ii) The probe configuration with

the laser beams coming from below was used to measure the horizontal velocity component (V).

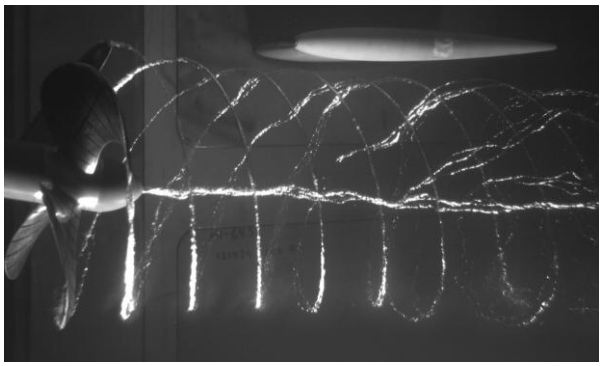

Figure 4. Visualization of unsteady interaction between the propeller tip and hub vortices in oblique flow (SINTEF Ocean)

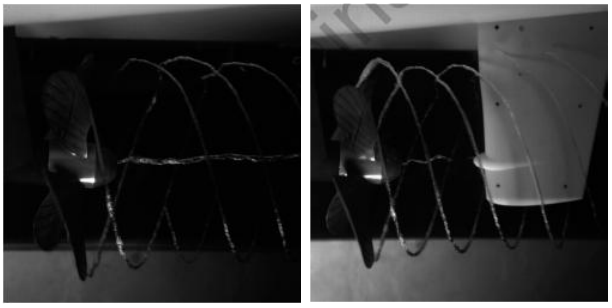

Figure 5. Influence of rudder bulb on the strength of propeller hub vortex. Left – setup w/o rudder; Right – setup with rudder (SINTEF Ocean)

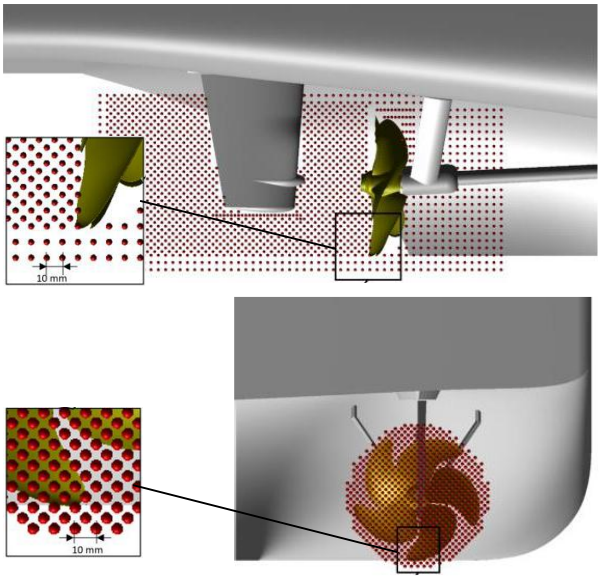

Figure 6. LDV measurement grids on the meridional and transverse sections of propeller slipstream

The LDV measurements were conducted in the four planes to acquire information about the velocity field in propeller slipstream: (i) Plane X0: meridional plane passing through propeller axis; (2) Plane X1: transversal plane (perpendicular to propeller axis) at x/D=0.37 (plane between the propeller plane and rudder axis); Plane X2: transversal plane at x/D=0.76 (at the rudder axis); Plane X3: transversal plane at x/D=1.30 (downstream of the rudder). The measurement grids consisted of 1652 points (plane X0), 783 points (planes X1 and X3) and 304 points (plane X2). Fig. 6 gives an appreciation of the LDV measurement grids.

2.2 CFD simulation techniques

This section describes the main features of the CFD simulation methods employed in ProNoVi to address the problem of propeller hydroacoustics. The main challenges associated with numerical modelling are related to: (i) resolution of highly anisotropic field of turbulence in the wake of ship hull and propeller slipstream; (ii) prediction of dynamic behaviour of cavitation on propeller blades and in propeller-induced vortices; (iii) solution of sound propagation in the ambient flow domain.

While used successfully in conventional open water and self-propulsion calculations, the RANS method shows serious limitations in the resolution of hull and propeller vorticity field. Insufficient accuracy of this method is the consequence of averaging the Navier-Stokes equations and excessive numerical diffusion caused by the assumption about isotropic pattern of turbulence employed by most of turbulence models of industrial use. As demonstrated in (Krasilnikov, 2019) and (Kimmerl et.al., 2021), the scale resolving techniques such as DES and LES allow to capture the important noise sources in propeller slipstream with high fidelity, provided sufficiently fine spatial and temporal discretization. (Krasilnikov, 2019) provides also some practical recommendations regarding the choice of cell size and time step for this type of analyses on marine propellers. The cell size requirements need to take into consideration not only the scale of turbulent eddies intended to be resolved, but also the size of cavitating bubbles which in turn depends on the type of cavitation. If applied to the whole region of propeller slipstream, these mesh requirements render simulation nearly unfeasible due to excessive computation demands. Therefore, adaptive mesh refinement (AMR) may be employed to resolve significant vortical structures locally based on for example vorticity magnitude criterion or its equivalent.

In the project ProNoVi, the studies on the application of scale resolving simulation techniques were carried out by SCHOTTEL who used the software HELYX-core, a derivative of the open-source CFD library OpenFOAM, and by SINTEF Ocean who used the commercial CFD software STAR-CCM+. The HELYX solution was based on the implicit Large Eddy Simulation (ILES) method (Van Terwisga et.al., 2009) which does not require additional turbulence transport equations and subgrid-scale model to be solved. The LES implementation in STAR-CCM+ was based on the Smagorinsky subgrid-scale model (Smagorinsky, 1963) with a modified Van Driest damping function enforced in the near wall regions (Balaras et.al., 1996). Compared to other implementations, this traditional version of the LES model in STAR-CCM+ was still found

to provide the most accurate prediction of propeller integral characteristics (thrust and torque) on a wide range of geometries and operation conditions, the quantities which are notoriously more difficult to compute accurately by LES. Another difficulty with the LES solution is related to its performance in the problem of ship hull flow where it tends to predict premature flow separation on the aftship and, generally, under-predict hull resistance which leads to an incorrect prognosis of ship's self-propulsion point. To overcome the two mentioned issues, the Improved Delayed Detached Eddy Simulation (IDDES) method was also applied by SINTEF Ocean in STAR-CMM+. The delay factor incorporated in this model enhances its ability to distinguish between the LES and RANS regions on meshes where spatial refinement could give rise to ambiguous behavior. The subgrid length-scale introduced in the IDDES includes a dependence on the wall distance which allows RANS solution to be used in a thin near-wall region (Shur et.al., 2008). In the IDDES approach, the DES formulation of the SST K-Omega model due to (Menter & Kuntz, 2002) is used which modifies the dissipation term in the transport equation for the turbulent kinetic energy based on the length-scale ratio. This formualtion supports the use of flow transion model (in low-Reyonlds number simulations such as those in model scale) and roughness modified wall functions where it gives results very close to the RANS method in propeller open water and hull resistance calculations. The described IDDES approach was successfully applied at SINTEF Ocean to full-scale ship self-propulsion simulations, showing generally a superior performance compared to RANS.

In the solution of the phase transfer problem required to predict cavitation, the Schnerr-Sauer cavitation model is used which is based on a reduced Rayleigh–Plesset equation and neglects the influence of bubble growth acceleration, viscous effects, and surface tension effects. This choice is primarily caused by the consideration of computational stability of the cavitation model at larger time steps. The scaling factors controlling the vaporization and condensation rates in the Schnerr-Sauer model were set to their default values of 1.0. The nuclei density was $1\times10^{12}(m^{-3})$ in both the HELYX and STAR-CCM+ implementations, while the nuclei diameter was 1×10^{-4}(m) and 1×10^{-6}(m), respectively.

Detailed verification and validation studies conducted by SCHOTTEL and SINTEF Ocean on commonly recognized open water benchmark propeller cases of PPTC and Newcastle propeller demonstrate that with the appropriate spatial and temporal resolutions both the LES and DES methods are capable of predicting propeller vortices and their cavitation with high fidelity, see for example (Krasilnikov, 2019) and (Kimmerl et.al., 2021).

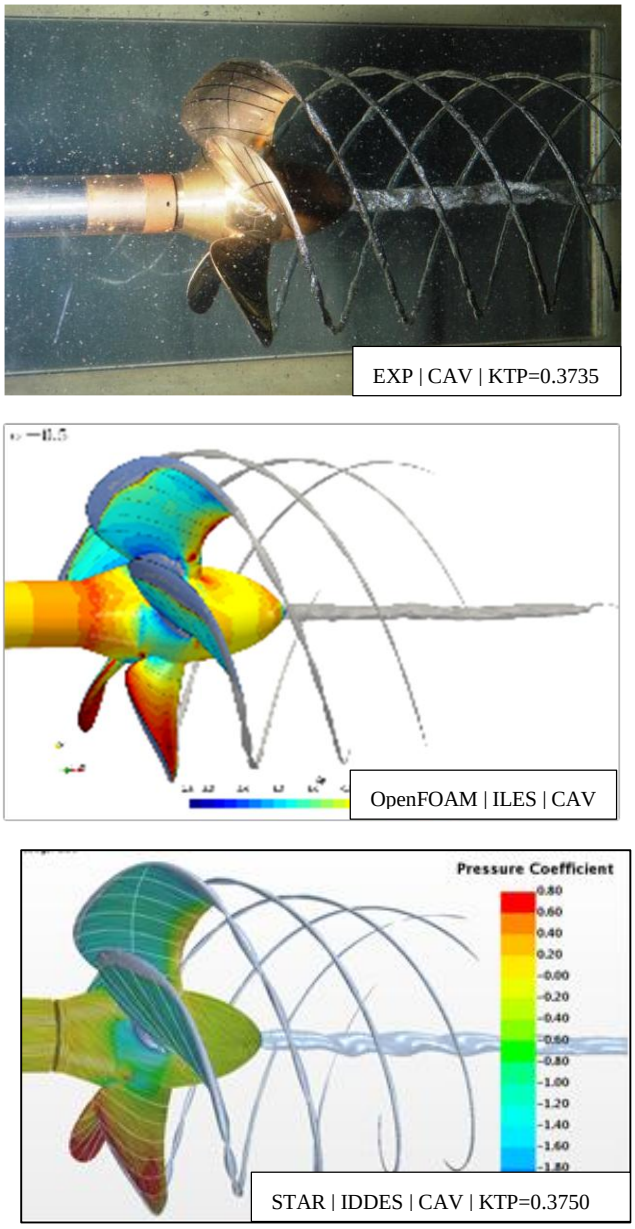

Figure 7. Prediction of cavitating propeller tip and hub vortices. PPTC propeller case in straight flow. J=1.019, σn=2.024.

An illustration of such predictions is given in Fig. 7. This level of accuracy comes at appreciable computation cost, and the use of AMR technique to track the vortices of interest is essential. The use of AMR is more problematic when propeller vortices become unstable. The vortex instability may originate from different causes, including oblique flow, interaction with rudder, or even interaction between the vortices themselves. An example of the latter type of interaction is shown in Fig. 8 for the propeller P3193 which is one of the target propeller cases investigated in ProNoVi. In this case, due to a special converging/diverging shape of hub cap (Condiv), the hub vortex is unstable in both the non-cavitating and cavitating conditions. However, without

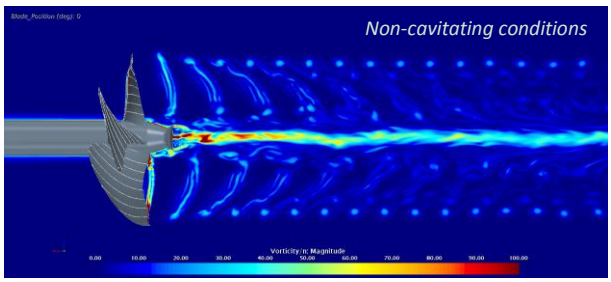

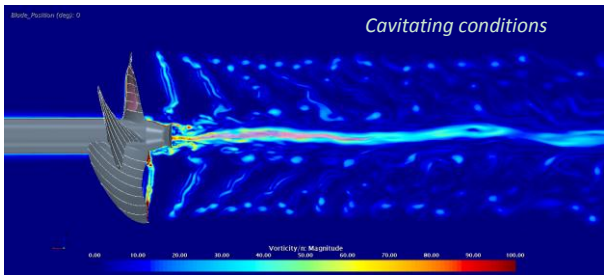

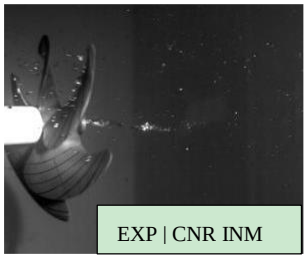

Figure 8. Influence of cavitating hub vortex on instability of blade tip vortex. Propeller P3193. Open water, straight flow, KT=0.192, σn=0.8. (STAR-CCM+ |LES| magenta areas show computed cavitation domains)

cavitation it does not have appreciable influence on the behavior of the tip vortex. Once cavitation in the hub vortex develops, a fluctuating pressure field disturbs the tip vortices making them unstable. This type of interaction is only captured by LES on a rather fine mesh applied in the whole domain of propeller slipstream (cell size in propeller slipstream 0.5% of propeller diameter; total cell count 54 million). In general, both the DES and LES techniques show comparable results regarding the hub vortex flow, but with the LES method one achieves a better resolution of the tip vortex and coarser grids.

Another aspect of practical relevance to propeller hydroacoustic simulations is related to the influence of sliding mesh interface on propagation of vorticity generated by the propeller. It is a common finding with both the OpenFOAM (Arbitrary Mesh Interface) and STAR_CCM+ (Sliding Mesh Interface) that such interfaces affect both the strength of the vortex and its shape as illustrated in Fig. 9. In the case of propeller in open water conditions, using a long propeller region extended downstream has clear advantages. However, this solution is not applicable in the case of propeller with rudder where other approaches such as for example Overset Mesh are required. In the example presented in Fig. 9, the cell size of 0.125% of propeller diameter was already sufficient to capture and maintain the core of

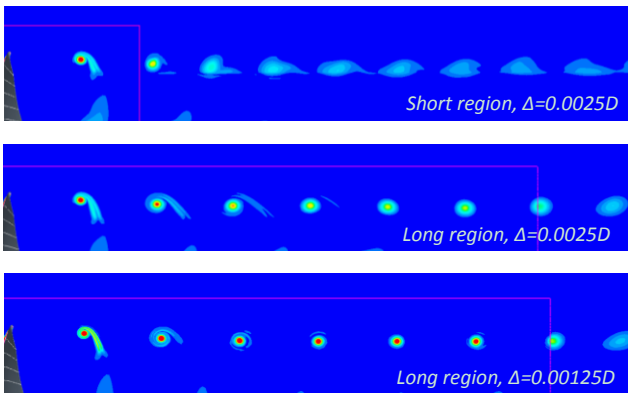

Figure 9. Influence of sliding mesh interface on the resolution of propeller tip vortex. PPTC propeller case in straight flow. J=1.268, σn=1.424. (STAR-CCM+ | LES | magenta line shows the contour of sliding mesh region)

of the tip vortex through the whole long propeller region. Occurrence of vapour phase in cavitating flow conditions affect the viscous vortex core and maintaining it in the solution becomes even more demanding. The results obtained with the Schnerr-Sauer cavitation model reveal dependency on the size of the nuclei diameter set in the model. This dependency is more pronounced in the scenarios featuring unsteady cavitation patterns such as the oblique flow conditions considered in Fig. 10.

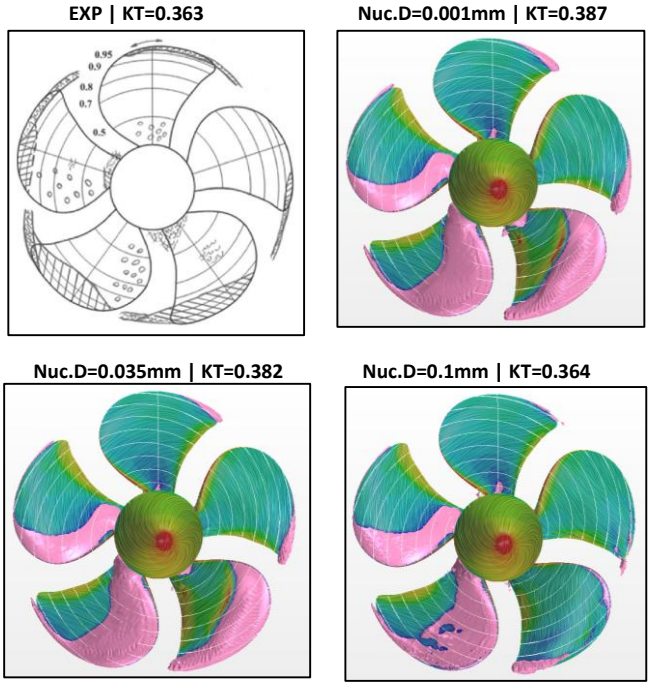

Figure 10. Influence of nuclei seed diameter on predicted propeller cavitation. PPTC propeller case in oblique flow of 12(deg). J=1.019, σn=2.024. (STAR-CCM+ | LES)

Obviously, the input diameter of nuclei affects both the cavitation pattern and computed propeller thrust. Using higher values yields predictions closer to the experimental data, but it also increases unsteady fluctuations of propeller forces, and more detailed investigations are required to

conclude whether these fluctuations are realistic. The mentioned solution dependency on the parameters of nuclei seed, and important role of bubble dynamics in the formation and development of cavitating vortices suggest that more accurate approaches may be needed to improve fidelity of numerical analyses, such as for example hybrid Eulerian-Lagrangian cavitation models that account for the contribution of individual bubbles (Lidtke, 2017).

Direct calculation of propeller radiated noise from the computed pressure field is only feasible in the near field. Already for medium-field direct calculations become overwhelming due to computational demand (mesh, time step) and hardly realistic due to neglection of flow compressibility. For these reasons, the methods based on the acoustic analogy are commonly employed, where the sound sources obtained from the hydrodynamic solution are reduced to the emitters distributed over control surfaces, and the equations of the fluid motion in the far field are recast in the form of an inhomogeneous wave equation. In the project ProNoVi, the most common acoustics integral method by Ffowcs Williams-Hawkings (FWH) is employed with both CFD solvers, following the Farassat's Formulation 1A (Brentner and Farassat, 1998). This method is based on a generalized Lighthill acoustic analogy which respects solid boundaries and uniform convection effects, and it is applied to compute noise at the far-field observer. The formulation is derived from the compressible Navier-Stokes equations under the assumption of a non-viscous medium, and it reduces the acoustic pressure sources to a non-deformable permeable control surface build around the relevant flow structures – the noise sources. Hence, this method is often referred under the abbreviation "P-FWH". The numerical solution takes into consideration the monopole/thickness, dipol-e/loading and quadrupole/volume terms. It employs signal pruning on the incomplete ends of the time interval, and time-lag between the emission and reception times. While in HELYX implementation, the evaluation of time signal is only carried out at run-time and only signals at pre-defined observers are reported, the two execution modes are supported in STAR-CCM+ – (i) the On-The-Fly mode identical to the above, and (ii) FWH-Post mode where the data on the emission surface are stored at all time steps and can subsequently be reused for any location of the observer. The permeable FWH surface can be constructed in the form of a cylinder or rectangular box surrounding the domain of hydrodynamic noise sources. The arrangement with a cylindrical FWH surface is shown in Fig. 11 for the case of propeller behind ship hull where it contains propeller with a part of its slipstream, rudder, and shaft support brackets upstream of propeller.

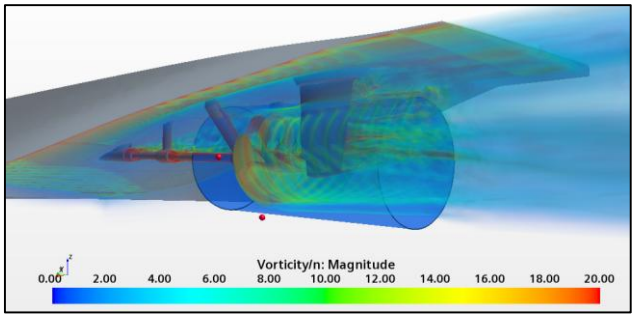

Figure 11. Arrangement of the permeable FWH surface around propeller operating behind ship hull. ProNoVi Reference Ship Case. (STAR-CCM+ | DES)

Comparisons between the different FHW implementations and direct calculation of sound pressure in the near field were carried out for the case of propeller in open water conditions. Fig. 12 shows the comparison involving the FWH On-The-Fly and FWH-Post formulations. Fig. 13 illustrates the influence of the shape and size of permeable FWH surface.

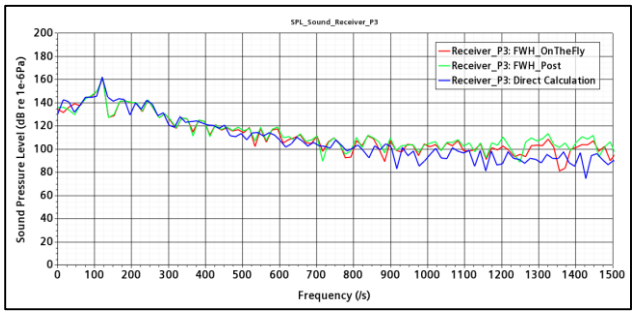

Figure 12. Comparison between the narrowband SPL distributions predicted from the direct noise calculation, FWH On-The-Fly and FWH-Post formulations. Propeller P1595 in open water, straight flow. J=0.6, σn=2.0. (STAR-CCM+ | LES)

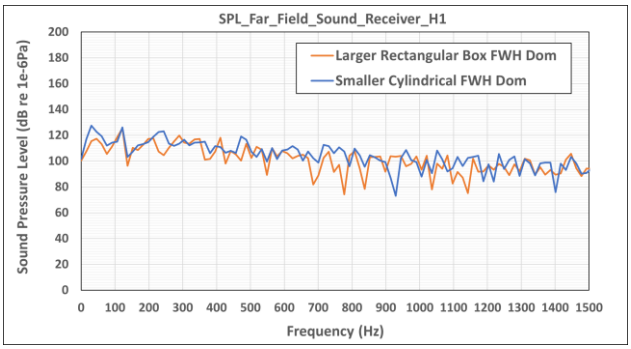

Figure 13. Influence of the shape and size of the FWH permeable surface. FWH On-The-Fly formulations. Propeller P1595 in open water, straight flow. J=0.6, σn=2.0. (STAR-CCM+ | LES)

3 VALIDATION DATASETS

In this section the validation datasets developed in ProNoVi are described. They include the two propeller models tested in open water conditions and behind hull of the reference target ship case, the twin-screw yacht by Lürssen. The main particulars of the two propellers are summarized in Table 1.

Table 1. Main particulars of propellers

Parameter	Units	P1595	P3193
Diameter	$[m]$	0.204	0.204
Pitch ratio	$[-]$	1.188	1.061
Blade area ratio	$[-]$	0.626	0.849
Skew	[°]	42	42
Number of blades	$[-]$	4	5
Hub ratio	$[-]$	0.196	0.196
Hub cap type		Elliptic	Condiv
Ship scale	$[-]$	21.0874	21.0784
Full-scale data		No	Yes
Distribution level		Open	Restricted

The open-geometry propeller P1595 was designed by SINTEF Ocean specifically for the purpose of the present test campaign to exhibit different types of cavitation. This is not the actual design for the reference ship case, since the main idea behind it has been to provide data on cavitation performance under different operation conditions. The general view of propeller P1595 is shown in Fig. 14.

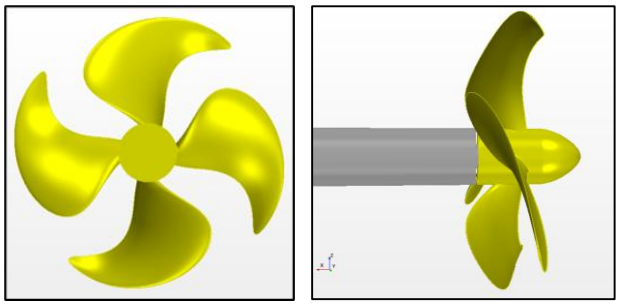

Figure 14. General view of the open-geometry propeller model P1595

Tables 2 and 3 present the scope of measurements performed on the two propeller models in open water conditions. Tables 4 and 5 present the scope of measurements with these propellers in behind hull conditions. The experimental results are documented in the ProNoVi test reports (Felli & Micci, 2021), (Nataletti, 2020) and (Kozlowska, 2020).

Table 2. Test matrix with propeller P3193 in open water (OW) conditions

Cond.	KT	Jv	$\sigma_{(nD)}$ (0.7R at 12 o'clock)	Shaft angles (deg)
OW-C1	0.192	0.755	Atm, 1.384, 0.9, 0.8	0, 2.75, 5.5, 11
OW-C2	0.267	0.6	Atm, 1.28, 0.9, 0.8	0, 2.75, 5.5, 11
OW-C3	0.116	0.9	Atm, 1.28, 0.9, 0.8	0, 2.75, 5.5, 11
Conducted tests (SINTEF Ocean and CNR INM): Cavitation observations, High-speed video, Cavitation bucket (SINTEF Ocean only), Noise				

Table 3. Test matrix with propeller P1595 in open water (OW) conditions

Cond.	KT	Jv	$\sigma_{(nD)}$ (0.7R at 12 o'clock)	Shaft angles (deg)
OW-C1	0.302	0.6	Atm, 3.0, 2.0, 1.5	0, 11
OW-C2	0.212	0.8	Atm, 0.92, 0.8, 0.72	0, 11
OW-C3	0.100	1.0	Atm, 1.48, 0.77	0
Conducted tests (SINTEF Ocean only): Cavitation observations, High-speed video, Cavitation bucket, Noise, Stereometry for selected conditions				

Table 4. Test matrix with propeller P3193 in behind hull (BH) conditions

Cond.	KT	Jv	$\sigma_{(nD)}$ (0.7R at 12 o'clock)	Rudder / angles (deg)
BH-C1	0.192	0.832	Atm, 1.384, 0.9	w/o, 0, 5
BH-C2	0.267	0.666	Atm, 1.20, 1.08	w/o, 0, 5
BH-C3	0.165	0.872	Atm, 4.94, 0.85	w/o, 0, 5
Conducted tests (SINTEF Ocean and CNR INM): Cavitation observations, High-speed video, Noise, Pressure pulses on hull, LDV velocity field (CNR INM only – BH-C1, Atm), Tests at 5(deg) rudder angle only at CNR INM Condition BH-C1 $\sigma_{(nD)}$=1.384 corresponds to full-scale noise measurements performed by Lürssen				

Table 5. Test matrix with propeller P1595 in behind hull (BH) conditions

Cond.	KT	Jv	$\sigma_{(nD)}$ (0.7R at 12 o'clock)	Rudder / angles (deg)
BH-C1	0.302	(0.6)	Atm, 2.0	w/o, 0
BH-C2	0.212	(0.8)	Atm, 0.8	w/o, 0
Conducted tests (SINTEF Ocean only): Cavitation observations, High-speed video, Noise, Pressure pulses on hull				

4 COMPARATIVE RESULTS

A very large volume of validation exercises with different numerical approaches have been carried out in ProNoVi using the experimental datasets described in Section 3.

Only selected results are presented in this paper, including: (i) noise levels and cavitation patterns on propeller P1595 in open water condition OW-C1; (ii) noise levels, hull pressure pulses and cavitation patterns on propeller P3193 in behind hull conditions BH-C2; (iii) vorticity field around propeller P3193 and experimental full-scale noise prognosis in behind hull condition BH-C1.

4.1 P1595 – Condition OW-C1

Fig. 15 shows a comparison between the sound pressure levels predicted with the LES method in STAR-CCM+ on the three systematically refined meshes and experimental measurements done at SINTEF Ocean. The experimental data are presented as 1/3 octave bands, while numerical results are presented as both the 1/3 octave bands and narrowband spectra. The frequency range in these examples is limited to 2000 (Hz) due to its higher relevance to both the observed phenomena and comparison with numerical simulations.

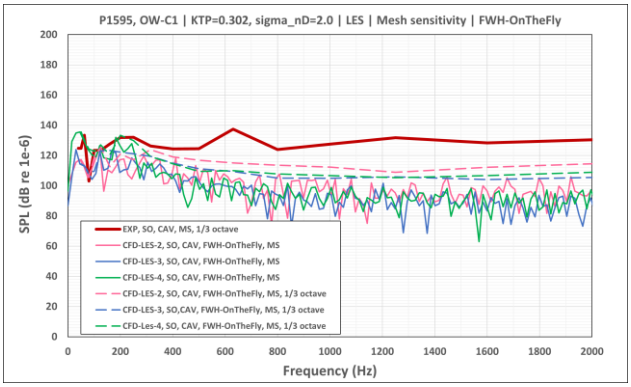

Figure 15. Comparison of computed and measured sound pressure levels. Mesh sensitivity. Propeller P1595 in open water, straight flow. J=0.6, σn=2.0. (STAR-CCM+ | LES)

These CFD simulations were performed using a quasi-infinite computation domain, without considering the presence of tunnel walls. The corresponding cavitation images are compared in Fig. 16. In the solution obtained on the finest grid LES-4 one can notice a dual tip vortex which

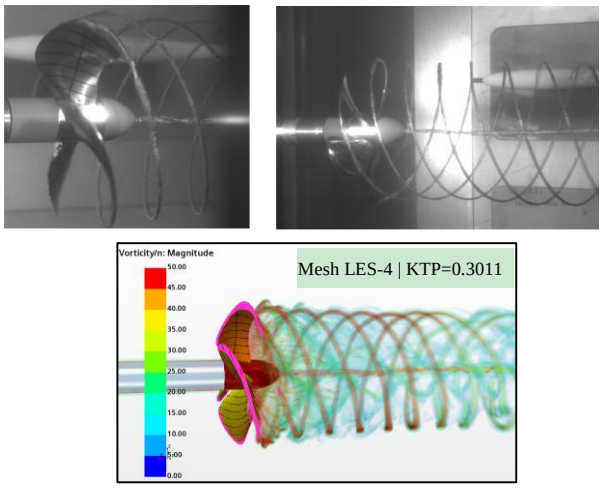

Figure 16. Comparison of computed and observed cavitation patterns. Propeller P1595 in open water, straight flow. J=0.6, σn=2.0. (STAR-CCM+ | LES | Mesh LES-4)

is also observed in the experiments on this propeller at J=0.6. However, even the finest mesh was not sufficient to resolve cavitation in the tip and hub vortices downstream of the propeller, which was also one possible reason for underprediction of noise level at higher frequencies seen in Fig. 15. Another factor contributing to the difference may be related to influence of cavitation tunnel environment. Otherwise, the numerical method provides a satisfactory prognosis of noise level in the relevant low frequency range (up to 300Hz), and the solution demonstrates convergence with mesh refinement. Fig. 17 present a comparison between the LES and IDDES solutions obtained on the medium mesh LES/DES-3 for the same condition.

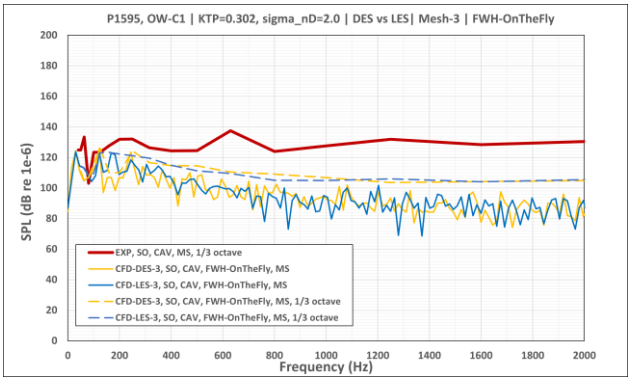

Figure 17. Comparison of computed and measured sound pressure levels. DES vs LES. Propeller P1595 in open water, straight flow. J=0.6, σn=2.0. (STAR-CCM+)

The sound pressure levels predicted by the two scale resolving simulations are found to be in close agreement, except that the LES method predicts higher level around the frequency of 200Hz which is closer to the measured data.

4.2 P3193 – Condition BH-C2

For this test condition of propeller P3193 behind ship hull comparisons were made between the two CFD simulations – OpenFOAM with the ILES method and STAR-CCM+ with the IDDES method – and experimental measurements done at the testing facilities of SINTEF Ocean and CNR INM. As in the previous case, the STAR-CCM+ DES simulation was performed in an unbounded domain, while OpenFOAM LES simulation considered the presence of tunnel walls. The CFD setups replicated model tests with half-ship model at SINTEF Ocean. Fig. 18 presents a comparison between the cavitation patterns on propeller blades and rudder observed at SINTEF Ocean tests and predicted from CFD simulations. Fig. 19 shows collective bar charts of the measured and computed pressure pulses at the locations of transducers P3, P4 and P10 on the hull, for the first four harmonics of blade passing frequency.

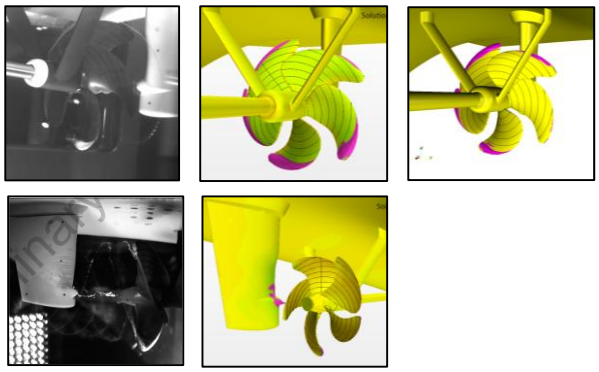

Figure 18. Comparison of observed and computed cavitation patterns on propeller and rudder. Propeller 3193 in behind hull conditions. KT=0.267, σn=1.2. (from left to right: Experiment, STAR-CCM+/DES, OpenFOAM/LES)

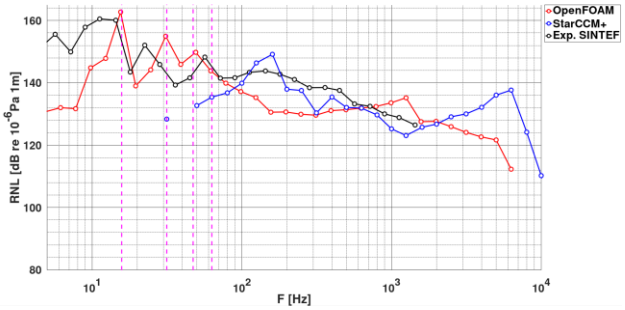

Figure 20. Comparison of computed and measured sound pressure levels. CFD solvers. Propeller 3193 in behind hull conditions. KT=0.267, σn=1.2.

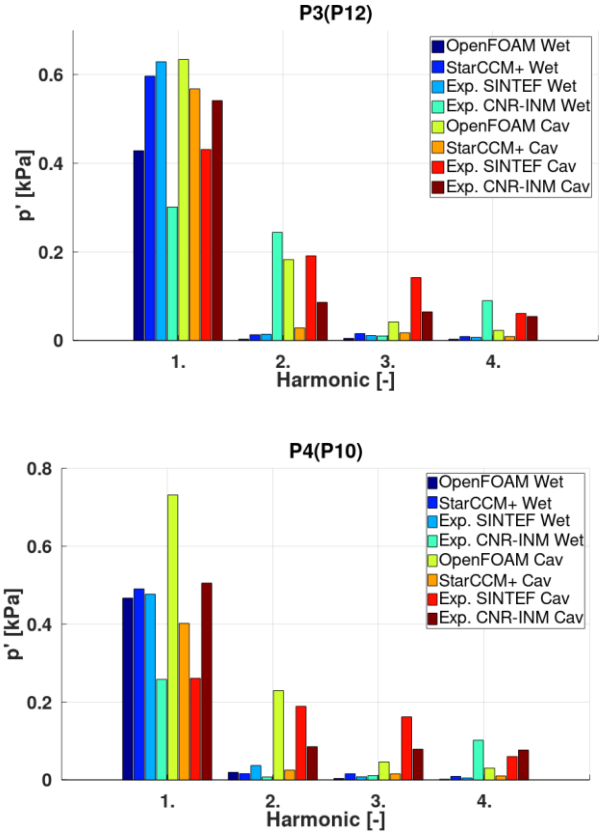

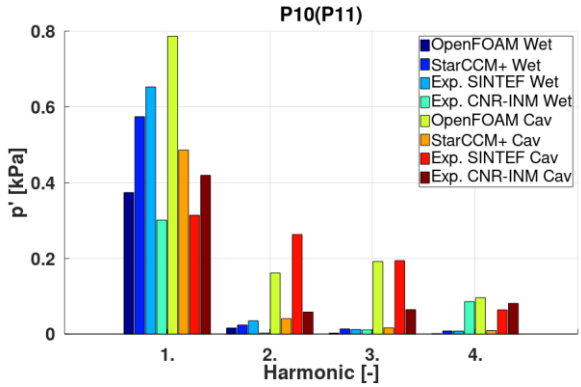

Figure 19. Measured and computed amplitudes of pressure pulses. Propeller 3193 in behind hull conditions. KT=0.267, Atm and σn=1.2. (Full scale values are sho-wn)

The pressure amplitudes were measured and computed in model scale and converted to full scale assuming the identity of dimensionless pressure coefficient $K_{PM}=K_{PS}$, $K_P=P/(\rho n^2D^2)$. The results are presented for both the non-cavitating and cavitating conditions. The measured and computed noise levels for the studied condition are compared in Fig. 20 in the format of 1/3 octave bands.

4.3 P3193 – Condition BH-C1

The comparative example presented for this condition concerns vorticity field in propeller slipstream. In Fig. 21, the contours of transversal vorticity field (ω_y) derived from the phase-locked LDV measurements conducted by CNR INM are compared in the meridional plane X0 with instantaneous contours of the same quantity obtained from the DES simulation in STAR-CCM+, at the respective positions of propeller blades. A similar comparison for the axial vorticity field (ω_x) is presented in Fig. 22 at the transverse planes X1 (between the propeller and rudder) and X3 (downstream of the rudder), for the portside and starboard, respectively.

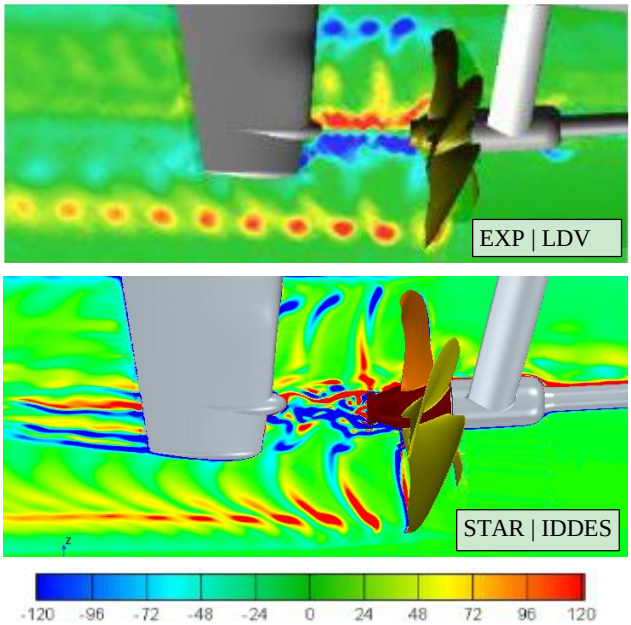

Figure 21. Comparison of contours of transversal vorticity (ω_x) on the meridional plane X0. Propeller 3193 in behind hull conditions. KT=0.192, Atm.

The analysis of these images reveals many common features in the measured and computed vorticity fields. The locations of the tip vortex cores and traces of blade vortex sheets in the planes X0 and X1 are in good agreement, while CFD simulations show more prolonged shape of the tip vortex core, which becomes distorted and more diffusive downstream of propeller region by the influence of sliding mesh interface. In the plane X3, downstream of the rudder, the vorticity field is dominated by the interacting rudder tip vortex and propeller hub vortex with four distinct area of increased vorticity magnitude. The rudder trailing vortex sheet is also clearly visible.

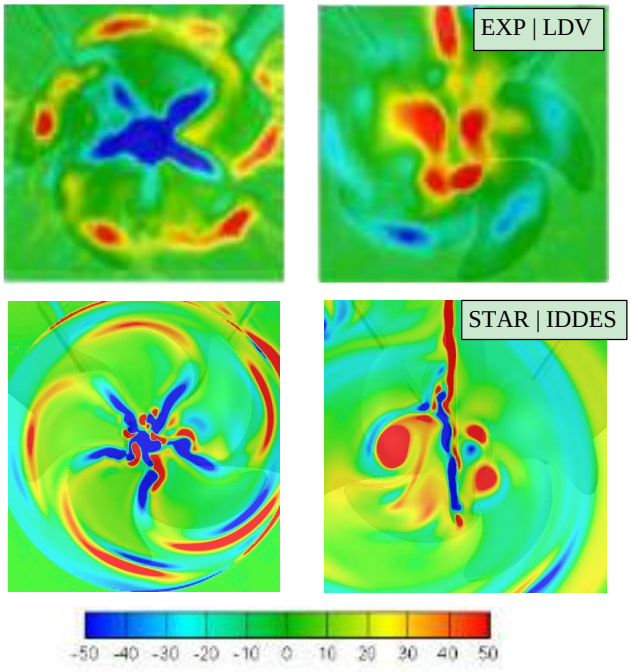

Figure 22. Comparison of contours of axial vorticity (ω_x) on the transverse planes X1 (left) and X3 (right). Propeller 3193 in behind hull conditions. KT=0.192, Atm.

For the same condition BH-C1, Fig. 23 shows a comparison between the full-scale noise prognoses made by the two testing facilities with the results of full-scale noise measurements on the reference ship performed by Lürssen.

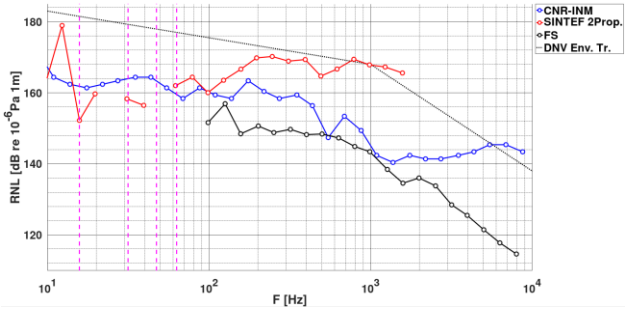

Figure 23. Predicted and measured full-scale noise levels for the reference ship at the test condition BH-C1 (FS refers to full-scale measurements; DNV environmental trend line is included for comparison)

5 CONCLUSIONS

Accurate prediction of propeller induced noise and vibrations remains a challenging task, concerning both the experimental and numerical methods. Validation of these methods should therefore continue. The approach adopted in ProNoVi where the same test conditions have been reproduced in full-scale, at different testing facilities and in different numerical environments is very useful for this purpose. Comparisons should comprise cavitation observations, pressure pulses, radiated noise and flow field. Such data are found, with carefully documented conditions, in the validation datasets developed in ProNoVi. Further efforts using these datasets will focus on more detailed comparisons in full-scale conditions.

Only by using Scale Resolving CFD simulations (DES, LES, SRH) one can achieve the degree of resolution required for propeller noise analyses. The DES and LES methods demonstrate generally comparable results in terms of cavitation on propeller blades and rudder, and in propeller hub vortex. Comparable pressure pulses and sound levels are predicted in these scenarios. LES methods show superior resolution of blade tip vortices, especially on coarser meshes, and better capabilities of capturing dynamic interaction between vortices. It is the cavitation in the tip vortex core downstream of propeller that is most demanding to resolve. This, and unsteady processes that accompany closure/collapse of blade cavitation, are seen as the primary factors responsible for larger differences between the measurements and calculations of noise and pressure fluctuations at higher frequencies.

Further efforts with CFD methods should focus on the improvements in LES/SRH near-wall capabilities, use of the Overset Mesh to overcome diffusive impact of sliding mesh interfaces, and Adaptive Mesh Refinement (AMR) procedures for unsteady scenarios. Since dynamics of individual cavitation bubbles plays an important role in formation and collapse of different types of cavitation, as well as their interaction, development and validation of hybrid Euler-Lagrange solutions are needed to eventually replace the VOF approach using cavitation models which hits its limits in the problem of propeller hydroacoustics.

ACKNOWLEDGEMENTS

The authors thank the partners in the ProNoVi project for the support of this work with their contributions to the discussion and the scientific exchange: SINTEF Ocean, CNR-INM, TUHH, Fr. Lürssen Werft GmbH & Co. KG, SCHOTTEL GmbH and Helseth AS. The authors are very grateful for the support and funding by MarTERA, represented by BMWi-project (03SX461C) “ProNoVi” for the German partners, the Research Council of Norway Project 284501 for the Norwegian Partners, and MIUR-project “ProNoVi” for the Italian partners.

REFERENCES

Balaras, E., Benocci, C., Piomelli, U. (1996). 'Two-Layer Approximate Boundary Conditions for Large-Eddy Simu-lations', AIAA Journal **34(6)**, pp. 1111-1119.

Cruz, E. Lloyd, T., Bosschers, J., Lafeber, F.H., Vinagre, P., Vaz, G. (2021). 'Study on inventory of existing policy, research and impacts of continuous underwater noise in Europe', EMSA report EMSA/NEG/21/2020. WavEC Offshore Renewables and Maritime Research Institute Ne-therlands.

Brentner, K. S. and Farassat, F. (1998). 'Analytical Comparison of the Acoustic Analogy and Kirchoff Formulation for Moving Surfaces', AIAA Journal, **36(8)**, 1998, p-p.1379-1386.

Felli, M. and Micci, G. (2021), 'Analysis Methods and Design Measures for the Reduction of Noise and Vibration In-duced by Marine Propellers. Deliverable D2 – CNR INM', CNR INM Report.

International Maritime Organization (IMO) (2014). 'Guidelines for the Reduction of Underwater Noise from Com-mercial Shipping to Address Adverse Impacts on Marine Life', London, Great Britain: IMO MEPC.1/Circ.833.

Kimmerl, J. et al. (2019). 'Analysis Methods and Design Measures for the Reduction of Noise and Vibration Induced by Marine Propellers', Proceedings of the 23rd International Congress on Acoustics, September 9-13, Aachen, Germany.

Kimmerl, J., Mertes, P., Abdel-Maksoud, M. (2021). 'Application of Large Eddy Simulation to Predict Underwater Noise of Marine Propulsors. Part 1: Cavitation Dynamics', Journal of Marine Science and Engineering, **9(8)**, 792.

Kozlowska, A.M. (2020). 'Cavitation Tests – 302004219', SINTEF Ocean Report OC2020 F-055, July.

Krasilnikov, V.I. (2019). ' CFD modelling of hydroacoustic performance of marine propellers: Predicting propeller cavitation', Proceedings of the 22nd Numerical Towing Tank Symposium NuTTS 2019, Tomar, Portugal, Sept 29 – Oct 1.

Lidtke, A.K. (2017). 'Predicting radiated noise of marine propellers using acoustic analogies and hybrid Eulerian-Lagrangian cavitation models', University of Southamp-ton, Doctoral Thesis, 237pp.

Menter, F. R. and Kuntz, M. (2002). 'Adaptation of Eddy Viscosity Turbulence Models to Unsteady Separated Flows Behind Vehicles', in The Aerodynamics of Heavy Vehicles: Trucks, Buses and Trains, Springer, Asilomar, CA.

Nataletti, M. (2020). 'ProNoVi EFD – Model tests', SINTEF Ocean Report 302004219, November.

Smagorinsky, J. (1963). 'General Circulation Experiments with the Primitive Equations: Part I, The Basic Experiment', Monthly Weather Review, **91**, pp. 99-164.

Shur, M.L., Spalart, P.R., Strelets, M.Kh., Travin, A.K. (2008). 'A hybrid RANS-LES approach with delayed-DES and wall-modelled LES capabilities', International Journal of Heat and Fluid Flow, **29(6)**, pp. 1638-1649.

Van Terwisga, T.J., Li, Z.R., Fitzsimmons, P.A., Foeth, E.J. (2009). 'Cavitation Erosion—A review of physical mechanisms and erosion risk models', Proceedings of the 7th International Symposium on Cavitation, Ann Arbor, MI, USA, 16–20 August.